Nanoscale magnetization and third-order nonlinearity by the plasmon-induced inverse Faraday effect in graphene-covered semiconductors

Chol-Song Ri,[1] Song-Jin Im [1,*] Ji-Song Pae,[1] Kum-Song Ho,[1] Yong-Ha Han,[1] and Joachim Herrmann[2,†]

[1]*Department of Physics, Kim Il Sung University, Taesong District, 02-381-4410 Pyongyang, Democratic People's Republic of Korea*
[2]*Max-Born-Institute for Nonlinear Optics and Short Pulse Spectroscopy, Max-Born-Strasse 2a, D-12489 Berlin, Germany*

In this paper we study an approach for nanoscale spatially inhomogeneous excitation of quasistatic magnetic fields by the plasmon-induced inverse Faraday effect (IFE) in graphene-covered semiconductors and we present analytical and numerical results for the induced magnetic field distribution. The effective magnetic field is predicted to reach about 1 T and the direction of the magnetic field can be switched by surface plasmon polaritons propagating into the opposite direction. By electrically controlling the chemical potential of the graphene sheet the spatial inhomogeneity of the magnetization near field can be broadly tuned. The response of the induced magnetization to the plasmon propagation is manifested by a nonlinear phase shift which is measurable in the far field. By using the Lorentz reciprocity theorem we analytically calculated the nonlinear susceptibility and the nonlinear absorption coefficient in dependence on the chemical potential, the frequency, and the other material parameters. The plasmon-induced IFE and the nonlinearity can be very strong by decreasing the chemical potential which is flexibly controllable by using the graphene's gate voltage. The studied system could pave the way for an alternative approach for nanometer spatial all-optical magnetization control.

I. INTRODUCTION

The inverse Faraday effect (IFE) provides a way for the generation of quasistatic magnetic fields in a magneto-optical material irradiated by free-space circularly polarized light. Recently this effect has attracted much attention due to its potential for ultrafast all-optical switching of magnetization [1–3] by ultrafast laser pulses, which opens a route for magnetic data storage with unprecedented speed. Magneto-optical effects can be enhanced in magnetoplasmonic structures due to the field enhancement by localized plasmon modes (for a review, see Refs. [4–9]). This method has also been used for field enhancement of the IFE by nanostructured gratings illuminated by free-space circularly polarized light [10–13]. The request to increase the recording density motivated studies for nanoscale-confined all-optical switching of magnetic films covered with gold double-wire antennas [14] and inside a magnetoplasmonic microcavity [15]. The spatial localization of coherent spin precession excitation within a magnetic plasmonic nanostructure has been studied in Ref. [16]. Recently we proposed a nanoscale version of all-optical magnetization switching by counterpropagating or two-frequency pulses using free-running surface plasmon polaritons (SPPs) [17]. The generation of magnetic fields by the IFE reacts to the plasmon propagation leading to a nonlinear phase shift due to a IFE-related third-order nonlinearity [18].

In the present paper we study the IFE induced by free-running SPPs in graphene-covered semiconductors for nanoscale spatially inhomogeneous excitation of magnetiza-

tion and its response to the SPP propagation manifested by a third-order nonlinearity. Wide applications for graphene in many fields have been found, in particular terahertz to mid-infrared applications [19–21]. SPPs supported by graphene-covered structures undergo better confinement and lower propagation loss compared to those by conventional metals such as gold and silver in the terahertz frequency range and are flexibly controllable by using the graphene's gate voltage [22]. Based on these advantages intensive and diverse studies on controllable graphene plasmonic devices have been reported (for a review, see Refs. [23,24]). In a recent study the possibility to control the distribution of the magnetic field due to the IFE in a graphene-dielectric-metal structure has been reported [25].

II. NANOSCALE MAGNETIZATION BY THE PLASMON-INDUCED INVERSE FARADAY EFFECT IN GRAPHENE-COVERED SEMICONDUCTORS

We consider the plasmonic propagations in two typical types of graphene-covered planar semiconductors as shown in Figs. 1(a) and 1(b).

The effect of an external magnetic field on surface plasmons in semiconductors has been studied theoretically [29] and experimentally [26]. Recently graphene plasmon modes in graphene-covered semiconductors have been intensively studied [30–34]. As shown in the previous studies, the permittivity tensor of the semiconductors in an external magnetic field H_{ext} in the direction of the y axis is expressed as

$$\hat{\varepsilon} = \begin{pmatrix} \varepsilon_1 & 0 & -ig \\ 0 & \varepsilon_\perp & 0 \\ ig & 0 & \varepsilon_1 \end{pmatrix}, \tag{1}$$

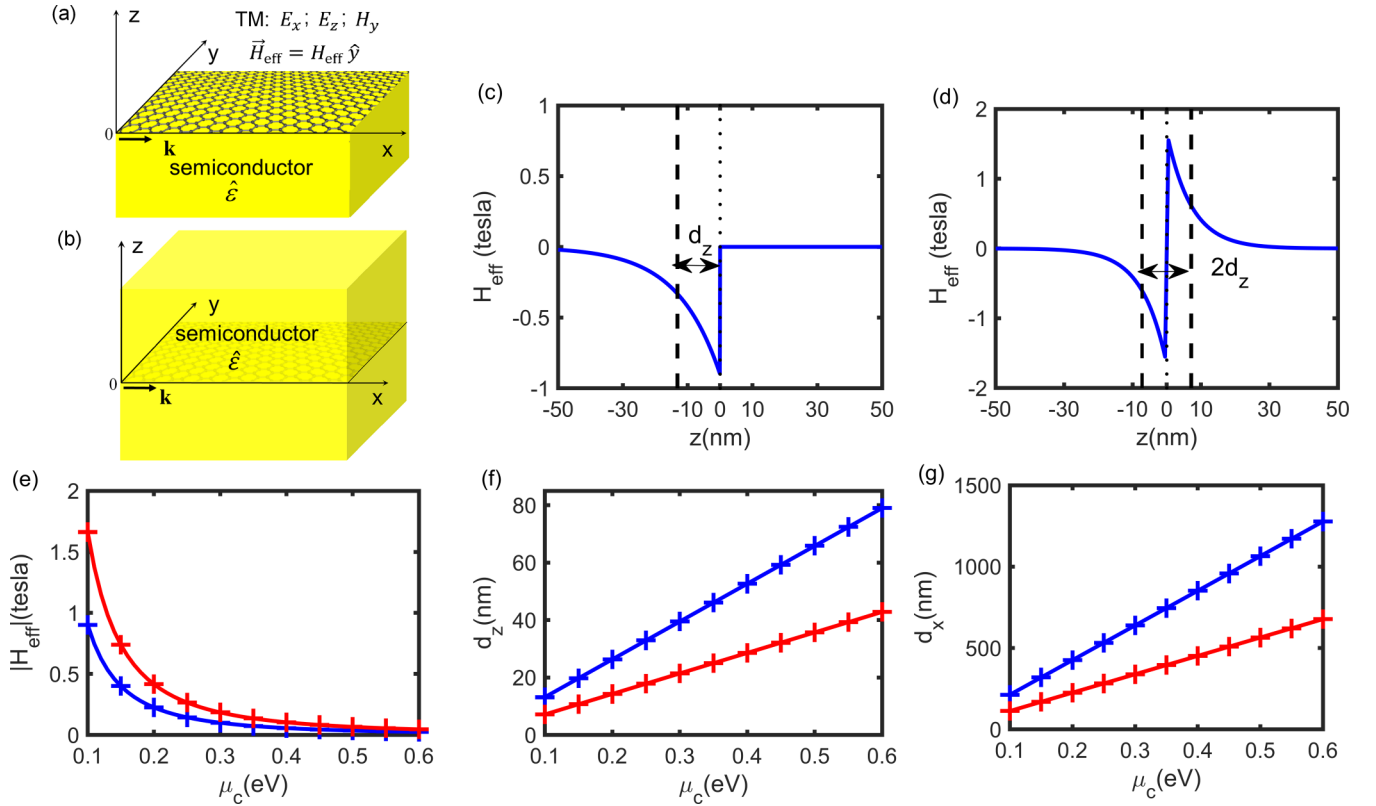*sj.im@ryongnamsan.edu.kp
†jherrman@mbi-berlin.de

FIG. 1. Nanoscale magnetization by the plasmon-induced IFE in graphene-covered semiconductors. Panels (a) and (b) show the schemes of two types of graphene-covered planar semiconductors: the graphene sheet surrounded by the air on one side and by a semiconductor on the other side (a) and the graphene sheet suspended in a semiconductor (b). Panels (c) and (d) show the transverse distributions of the effective magnetic field H_{eff} in the graphene-covered planar semiconductors at a chemical potential of $\mu_c = 0.1$ eV. Panels (c) and (d) correspond to panels (a) and (b), respectively. (e) The peak strength of the effective magnetic field at the interface versus the chemical potential for a mode power of 0.1 W/μm. Panels (f) and (g) show the $1/e$ decaying lengths of the effective magnetic field versus the chemical potential in the directions of the z axis (f) and the x axis (g). The blue and the red curves and crosses are for the cases of panels (a) and (b), respectively. The crosses have been calculated by Eq. (3) and numerical solutions of the dispersion relations of the transverse (TM) graphene plasmon mode (see the dispersion relation in Appendix A). The curves have been obtained by using the analytical formulas (4)–(6). We used $\varepsilon_1' = 11.8$ and $\alpha = 6 \times 10^{-7}$ m/A for the n-type InSb [26] at a frequency 10 THz. We assumed $\tau = 1/0.09\omega_p = 0.35$ ps as the carrier relaxation time of graphene. We note that values from 0.1 ps [27] to 1 ps [28] of τ are experimentally achievable at room temperature.

where

$$\varepsilon_1 = \varepsilon_\infty \left\{ 1 - \frac{\omega_p^2(\omega + i\gamma_s)}{\omega\left[(\omega + i\gamma_s)^2 - \omega_c^2\right]} \right\},$$

$$\varepsilon_\perp = \varepsilon_\infty \left[1 - \frac{\omega_p^2}{\omega(\omega + i\gamma_s)} \right],$$

$$g = \varepsilon_\infty \frac{\omega_p^2 \omega_c}{\omega\left[(\omega + i\gamma_s)^2 - \omega_c^2\right]}.$$

Here ω_p is the plasma frequency; $\omega_c = e\mu_0 H_{\text{ext}}/m_{\text{eff}}$ is the cyclotron frequency, with e being the charge and m_{eff} the effective mass of the electron, respectively; ε_∞ is the background permittivity, which depends on the properties of the bound electrons in the material; γ_s is the electron collision frequency responsible for the material absorption. The off-diagonal component of the permittivity tensor $g = \alpha H_{\text{ext}}$ is proportional to the external magnetic field, which means that the permittivity of semiconductors is formally similar to that in a magneto-optical medium. Its magneto-optical susceptibility

has a great value when ω is comparable with ω_p. As an example, for the n-type InSb with $\varepsilon_\infty = 15.68$, $\omega_p = 3.14 \times 10^{13}$ rad/s, $\gamma_s = 0.11\omega_p$, and $m_{\text{eff}} = 0.022m_e$, where m_e is the electron's mass [26], at a frequency of 10 THz corresponding to $\omega/\omega_p = 2$, the magneto-optical susceptibility has a value of $\alpha = 6 \times 10^{-7}$ m/A which is of the order of the values in typical magnetic materials; for example, the magneto-optical susceptibility of Bi-substituted iron garnet has a value of $\alpha = 5.5 \times 10^{-7}$ m/A [12] at a wavelength near 800 nm and has drastically smaller values at longer wavelengths [35]. The infinite thin graphene layers exhibit a surface conductivity σ. Since at room temperature the photon energy in the mid-infrared wavelength range is always less than $2\mu_c$ and the intraband transition dominates the interband transition, σ can be expressed by [36]

$$\sigma \approx ie^2\mu_c/[\pi\hbar^2(\omega + i/\tau)], \qquad (2)$$

where μ_c, $\hbar$, ω, and τ are the chemical potential, the reduced Planck's constant, the optical angular frequency, and the carrier relaxation time, respectively. The quasistatic magnetic field along the y direction parallel to the graphene sheet has no

direct interaction with the graphene and directly modulates the semiconductor's optical property as shown in Eq. (1), while in the case that it is in the direction perpendicular to the graphene sheet the graphene's optical property is directly modulated [37].

Due to the inverse Faraday effect an effective magnetic field is generated which is described by

$$\vec{H}_{\text{eff}} = -i\varepsilon_0\alpha\vec{E} \times \vec{E}^*, \tag{3}$$

where ε_0 is the vacuum permittivity and α is the above-given magneto-optical susceptibility. The rotating electric field vector of the SPP propagating in the graphene-covered planar semiconductors exhibits a longitudinal component. Therefore the vector product in Eq. (3) is nonzero and a quasistatic magnetic field along the y direction in Figs. 1(a) and 1(b) is generated.

Due to the strong confinement in the graphene waveguide the relation $k \approx k_1 \approx k_2$ can be derived. Here, k is the graphene plasmon wave number and k_1 and k_2 are the wave-vector components perpendicular to the interface in the ε_1 side and the ε_2 side, respectively. In the zero-order approximation with respect to the magneto-optical effect

$$k \approx k_1 \approx k_2 \approx \frac{\pi\hbar^2\omega^2\varepsilon_0(\varepsilon_1+\varepsilon_2)[1+i/(\tau\omega)]}{e^2}\frac{1}{\mu_c}.$$

By using the TM modes of the SPPs in the graphene waveguide we derive the following analytical formulas for the IFE-induced effective magnetic field (see the detail derivation in Appendix A):

$$H_{\text{eff}}/P \approx \sigma_p\frac{8\pi^2\hbar^4\alpha\varepsilon_0^2\omega^3(\varepsilon_1'+\varepsilon_2')}{e^4}(\mu_c)^{-2}$$
$$\times \exp\left(-x/d_x\right)\exp\left(-|z|/d_z\right), \tag{4}$$

$$d_z \approx \frac{e^2}{2\pi\hbar^2\varepsilon_0\omega^2(\varepsilon_1'+\varepsilon_2')}\mu_c, \tag{5}$$

$$d_x \approx \frac{e^2}{2\pi\hbar^2\varepsilon_0\omega^2(\varepsilon_1'+\varepsilon_2')}$$
$$\times \frac{1}{[1/(\omega\tau)+(\varepsilon_1''+\varepsilon_2'')/(\varepsilon_1'+\varepsilon_2')]}\mu_c. \tag{6}$$

Here $\sigma_p = s_1 \cdot s_2$, where $s_1 = \hat{x} \cdot \hat{k} = \pm 1$ and $s_2 = \hat{z} \cdot \hat{s} = \pm 1$. $\hat{k}$ is the unit vector along the propagation direction of the graphene plasmon and $\hat{s}$ the unit normal vector of the graphene sheet directed from the graphene sheet to a semiconductor side. $\hat{x}$ and $\hat{z}$ are the unit vectors along the x and z axes, respectively. $P = |\int 1/2\text{Re}(\vec{E}^* \times \vec{H})\hat{x}dz|$ is the mode power of the graphene plasmon at $x = 0$. ε_2 is the permittivity of the upper medium, and $\varepsilon_2 = 1$ in Fig. 1(a) and $\varepsilon_2 = \varepsilon_1$ in Fig. 1(b). ε' and ε'' mean the real and imaginary parts of the complex value ε, respectively, and d_z and d_x are the $1/e$ decaying lengths of the effective magnetic field in the directions of the z axis and the x axis, respectively. Figures 1(c) and 1(d) show the near field distributions of the effective magnetic field which is tightly confined near the graphene sheet due to the strong confinement of the graphene plasmons. Figures 1(e)–1(g) show the effective magnetic field [panel (e)] and the decay lengths d_z [panel (f)] and d_x [panel (g)] of the effective magnetic field which are broadly tunable

by changing the chemical potential. As seen the magnetic field reaches values in the range of 1 T for a chemical potential of 0.1 eV. The magnetic field decreases with increasing μ_c because the decay length d_z is proportional to the surface conductivity of graphene σ (see Appendix A) and thus is proportional to the chemical potential μ_c [see Eq. (2)], and the smaller value of d_z results in the larger magnitude of $\vec{E}$ for the same mode power. We note that the chemical potential is electrically controllable in practice by using a gate voltage of the graphene sheet. The simple and explicit dependence of the effective magnetic field on the chemical potential, as shown in the analytical formulas (4)–(6), agrees with the numerical results [the crosses of Figs. 1(e)–1(g)] which have been calculated by Eq. (3) and the numerical solutions of the electric field of the transverse (TM) graphene plasmon mode. As seen in Eq. (4) the sign of H_{eff} is determined by the sign of $s_1 = \hat{x} \cdot \hat{k} = \pm 1$ and can be reversed by the change of the SPP propagation direction. In contrast to switching the direction of the magnetic field by the helicity of free-space circularly polarized pulses, the direction of the magnetic field in the plasmon-induced IFE is determined by the SPP propagation direction [17].

III. THIRD-ORDER NONLINEARITY BY THE PLASMON-INDUCED INVERSE FARADAY EFFECT IN GRAPHENE-COVERED SEMICONDUCTORS

The effective magnetic field in the magneto-optical material induces the off-diagonal component of the permittivity tensor $g = \alpha H_{\text{eff}}$, where H_{eff} is the magnetic field due to the plasmon-induced IFE [17,18]. Consequently, it leads to a wave-number shift of the TM graphene plasmon mode and therefore to a IFE-related third-order nonlinearity [18] which differs from the optical Kerr effect. By substituting the unperturbed backward-propagating field and the perturbed forward-propagating field under the effective magnetic field in the Lorentz reciprocity theorem [38], we derived an analytical formula for the nonlinear complex-valued susceptibility γ (see the detail derivation in Appendix B):

$$\gamma \approx \frac{4\pi^3\hbar^6\varepsilon_0^4c^2\alpha^2\omega^5}{e^6}(\varepsilon_1'+1)$$
$$\times \left[1+i\left(\frac{3}{2\omega\tau}+\frac{\varepsilon_1''}{\varepsilon_1'+1}\right)\right](\mu_c)^{-3} \tag{7}$$

for the scheme of Fig. 1(a) and

$$\gamma \approx \frac{16\pi^3\hbar^6\varepsilon_0^4c^2\alpha^2\omega^5}{e^6}\varepsilon_1'$$
$$\times \left[1+i\left(\frac{3}{2\omega\tau}+\frac{\varepsilon_1''}{\varepsilon_1'}\right)\right](\mu_c)^{-3} \tag{8}$$

for the scheme of Fig. 1(b). The real part of the nonlinear susceptibility γ' describes a nonlinear wave-number shift (or a nonlinear refraction index change) and the imaginary part of the saturable absorption of the TM graphene plasmon mode. In Fig. 2(a) the curves represent $\phi_{\text{NL}} = \gamma'P_{\text{in}}L_{\text{eff}}$ with the analytical formulas (7) and (8), where $L_{\text{eff}} = [1-\exp(-2k''L)]/(2k'')$. The analytical results are in good agreement with the numerically calculated phase shift $\phi_{\text{NL}} = \phi(P_{\text{in}} = P) - \phi(P_{\text{in}} \rightarrow 0)$ [the circles in Fig. 2(a)], obtained
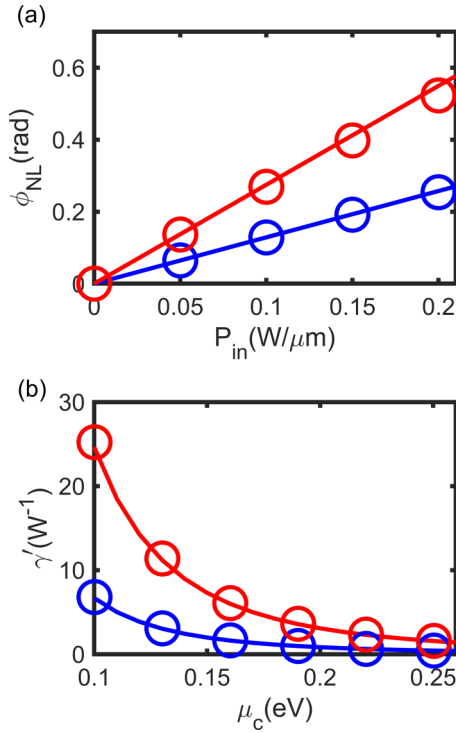
(a)

(b)

(a)

(b)

FIG. 2. Third-order nonlinearity due to the plasmon-induced IFE. (a) The nonlinear phase shift ϕ_{NL} at a propagation length of $L = 500$ nm versus the incident mode power P_{in}. (b) The dependence of the real part of the nonlinear coefficient γ' on the chemical potential μ_c. The blue and the red curves and crosses are for the cases of Figs. 1(a) and 1(b), respectively. The curves have been obtained by using the analytical formulas (7), (8), and $\phi_{NL} = \gamma' P_{in} L_{eff}$, where $L_{eff} = [1 - \exp(-2k''L)]/(2k'')$. The circles are calculated from the entity $\phi_{NL} = \phi(P_{in} = P) - \phi(P_{in} \to 0)$ and $\gamma = [k(P) - k(0)]/P$ calculated by numerical solutions of the Maxwell equation in the frequency domain. Other parameters are the same as those in Fig. 1.

by numerical solutions of the Maxwell equation in the frequency domain. The explicit dependence of the nonlinear coefficient γ' on the chemical potential [the curves in Fig. 2(b)], predicted in the analytical formulas (4) and (5), well agrees with the numerical results of $\gamma = [k(P) - k(0)]/P$ [the circles in Fig. 2(b)]. In the numerical simulations the graphene layer was treated as a very thin metal film with a thickness of $\Delta = 1$ nm and the equivalent bulk permittivity $\varepsilon_g = 1 + i\sigma\eta_0/(k_0\Delta)$, which has been widely validated [39,40]. More detail values from the simulation results can be seen in Table I.

TABLE I. Values of the frequency f in THz, the propagation length $1/2k''$ in μm, the electric field strength in the graphene sheet along the direction parallel to the graphene sheet E in V/m, the effective magnetic field H_{ext} in T, the graphene-plasmon wave number k' in $1/\mu$m, and the nonlinear wave-number shift $\Delta k'$ in $1/\mu$m for $P = 0.1$ W/μm and $\mu_c = 0.1$ eV.

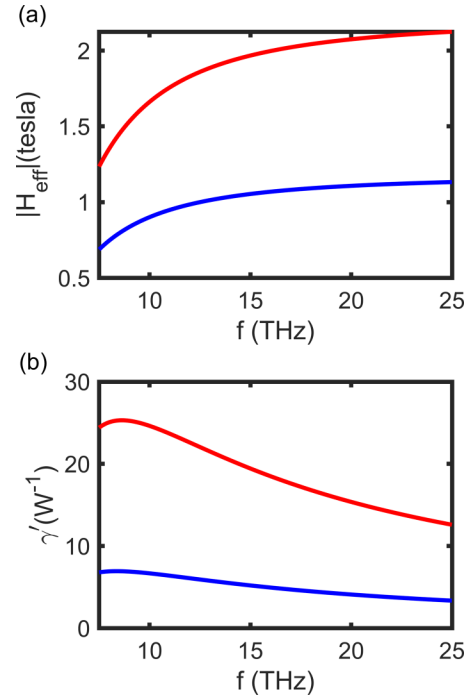|	f	$1/2k''$	E	H_{eff}	k'	$\Delta k'$
Fig. 1(a)	10	0.21	4.0×10^8	0.90	38	0.67
Fig. 1(b)	10	0.11	5.5×10^8	1.66	70	2.46

FIG. 3. Frequency dependency of the effective magnetic field (a) and the real part of the nonlinear coefficient (b) due to the plasmon-induced IFE. The blue and the red curves are for the cases of Figs. 1(a) and 1(b), respectively. The curves have been obtained by using the analytical formulas (4), (7), and (8) where the frequency-dependent permittivity tensor of the n-type InSb [26] is used for ε_1 and α. A chemical potential of $\mu_c = 0.1$ eV for panels (a) and (b) and a mode power of 0.1 W/μm for panel (a) have been assumed.

The effective magnetic field in Eq. (4) is proportional to the third power of the frequency, but this dependence is compensated by the strong frequency dependency of α which is inversely proportional to the third power of the frequency in semiconductors [26]. Figure 3(a) shows the effective magnetic field does not strongly depend on the frequency and is almost constant in the higher frequency range. The weak frequency-dependency is only due to the frequency dependency of ε_1 which becomes significant in the lower frequency range approaching the plasma frequency $f_p = \omega_p/(2\pi) = 5$ THz. Figure 3(b) shows the real part of the nonlinear coefficient γ' decreases with increasing the frequency because γ' is proportional to the second power of α. γ' has a maximum near a frequency of 10 THz and smaller values at lower frequencies attributed to the decrease of ε_1 with decreasing frequencies.

In the graphene-covered semiconductors a huge nonlinear coefficient γ of the order of 10 W^{-1} is achievable at $\mu_c = 0.1$ eV. For a mode power of $P = 0.1$ W/μm, $\Delta k = \gamma P$ is of the order of 0.1 μm^{-1}, which is about 2 or 3 orders of magnitude larger than Δk_{mp} in Ref. [6] and $\Delta k = \gamma P$ in Ref. [18].

IV. DISCUSSION AND CONCLUSIONS

We investigated nanoscale spatially inhomogeneous excitation of quasistatic magnetic fields by the plasmon-induced IFE in graphene-covered semiconductors. Enhancement of

the plasmon-induced IFE is attributed to tight transverse confinement of the graphene plasmon and the slow light effect due to a huge effective refractive index of the graphene plasmon which are in dependence on the chemical potential μ_c of the graphene sheet. The derived analytical formula explicitly shows that the induced magnetic field is inversely proportional to the square of the chemical potential μ_c which is flexibly controllable by using the graphene's gate voltage. For example, by changing μ_c from 1 to 0.1 eV, the induced magnetic field is enhanced by 100 times and can reach values of about 1 T for a mode power of 0.1 W/μm. The IFE-induced magnetic field is strongly confined near the surface of the graphene sheet. The sign of the magnetic field is reversed for counterpropagating SPPs. By electrically controlling the chemical potential of the graphene sheet the magnitude and the spatial shape of the magnetization near field can be broadly tuned. If a magnetized nanoscale material is placed near the graphene sheet, its magnetization can be controlled and switched into the opposite direction. The plasmon-induced magnetic field leads to a reaction to the SPP propagation by a third-order nonlinear effect which differs from the traditional optical Kerr effect. We derived an analytical formula for the IFE-related nonlinear susceptibility which is inversely proportional to the third power of the chemical potential. The numerical estimation of the nonlinear susceptibility predicts a huge value which is orders of magnitude larger than those of gold/ferromagnet structures. The huge value of the IFE-related nonlinear susceptibility at a small value of the chemical potential is attributed to enhancement of magnetoplasmonic effect under the enhanced IFE in the graphene-covered semiconductors. The predictions by the analytical formulas are in good agreement with the numerical solution of Maxwell equation in the frequency domain. The studied approach for nanoscale magnetization by the plasmon-induced IFE in graphene-covered semiconductors could pave the way for an efficient method for all-optical magnetization switching in nanometer-scale systems.

APPENDIX A: DERIVATIONS OF EQS. (4)–(6)

We consider the plasmonic propagations in two typical types of graphene-covered planar semiconductors as shown in Figs. 1(a) and 1(b). The permittivity tensor of the semiconductor in a magnetic field in the direction of the y axis is expressed by Eq. (1). The graphene surface conductivity σ can be expressed by Eq. (2). The rotating electric field vector of circularly polarized light induces an effective magnetic field along the wave vector $\vec{k}$, which is called the inverse Faraday effect (IFE). The rotating electric field vector of

TM graphene plasmon modes in the graphene-covered planar semiconductors can act as an effective magnetic field along the transverse y direction. In the zero-order of perturbation in $\alpha H_{\text{ext}}/\varepsilon_1$, the TM graphene plasmon modes are expressed as

$$H_{y2} = A_2 \exp(ikx) \exp(-k_2 z),$$
$$E_{x2} = iA_2(\eta_0 k_2/\varepsilon_2 k_0) \exp(ikx) \exp(-k_2 z), \quad \text{(A1)}$$
$$E_{z2} = -A_2(\eta_0 k/\varepsilon_2 k_0) \exp(ikx) \exp(-k_2 z),$$

for $z > 0$, and

$$H_{y1} = A_1 \exp(ikx) \exp(k_1 z),$$
$$E_{x1} = -iA_1(\eta_0 k_1/\varepsilon_1 k_0) \exp(ikx) \exp(k_1 z), \quad \text{(A2)}$$
$$E_{z1} = -A_1(\eta_0 k/\varepsilon_1 k_0) \exp(ikx) \exp(k_1 z),$$

for $z < 0$. Here η_0 is the vacuum wave impedance. ε_2 is the permittivity of the upper medium, and $\varepsilon_2 = 1$ in Fig. 1(a) and $\varepsilon_2 = \varepsilon_1$ in Fig. 1(b). From the requirement of the continuity of E_x and H_y at the graphene layer $z = 0$ ($E_{x1} = E_{x2}$ and $H_{y1} - H_{y2} = \sigma E_{x1}$),

$$\frac{A_1}{A_2} = -\frac{\varepsilon_1 k_2}{\varepsilon_2 k_1}, \quad \text{(A3)}$$

$$A_2 = \left(1 + \frac{i\sigma \eta_0 k_1}{k_0 \varepsilon_1}\right) A_1. \quad \text{(A4)}$$

Combining the above equations, we can get the dispersion relation as follows:

$$\frac{\varepsilon_1}{k_1} + \frac{\varepsilon_2}{k_2} + \frac{i\eta_0 \sigma}{k_0} = 0. \quad \text{(A5)}$$

From Eq. (3) and the fact that the TM graphene plasmon mode is under investigation, we find

$$H_{\text{eff}} = -i\varepsilon_0 \alpha (E_x^* E_z - E_x E_z^*). \quad \text{(A6)}$$

By substituting Eqs. (A1)–(A3) into Eq. (A6), we get

$$H_{\text{eff}} = \sigma_p \frac{2\alpha |A_1|^2 (k'k_1' + k''k_1'')}{\omega^2 \varepsilon_0 |\varepsilon_1|^2} \exp(-2k''x) \exp(-2k_1'|z|).$$

Here $\sigma_p = s_1 \cdot s_2$, where $s_1 = \hat{x} \cdot \hat{k} = \pm 1$ and $s_2 = \hat{z} \cdot \hat{s} = \pm 1$. $\hat{k}$ is the unit vector along the propagation direction of the graphene plasmon, and $\hat{s}$ is the unit normal vector of the graphene sheet directed from the graphene sheet to a semiconductor side under the investigation. $\hat{x}$ and $\hat{z}$ are the unit vectors along the x and z axes, respectively. We note that a' and a'' mean the real and the imaginary parts of the complex value a, respectively. From Eqs. (A1), (A2), and (A3), the mode power at $x = 0$ P is

$$
\begin{aligned}
P &= \left| \int 1/2 \text{Re}(\vec{E} \times \vec{H}^*)\hat{x} dz \right| = \left| \int 1/2 \text{Re}(E_z H_y^*) dz \right| = \frac{|A_1|^2 \text{Re}(\varepsilon_1 k)}{2\omega \varepsilon_0 |\varepsilon_1|^2} \int_{-\infty}^{0} \exp(2k_1' z) dz + \frac{|A_2|^2 \text{Re}(\varepsilon_2 k)}{2\omega \varepsilon_0 |\varepsilon_2|^2} \int_{0}^{\infty} \exp(-2k_2' z) dz \\
&= \frac{|A_1|^2 \text{Re}(\varepsilon_1 k)}{4\omega \varepsilon_0 |\varepsilon_1|^2 k_1'} + \frac{|A_2|^2 \text{Re}(\varepsilon_2 k)}{4\omega \varepsilon_0 |\varepsilon_2|^2 k_2'} = \frac{|A_1|^2 \text{Re}(\varepsilon_1 k)}{4\omega \varepsilon_0 |\varepsilon_1|^2 k_1'} + \frac{|A_2|^2 \text{Re}(\varepsilon_2 k)}{4\omega \varepsilon_0 |\varepsilon_2|^2 k_2'} \\
&= \frac{|A_1|^2}{4\omega \varepsilon_0 |\varepsilon_1|^2} \frac{k_2'(\varepsilon_1' k' - \varepsilon_1'' k'')(k_2'^2 + k_2''^2) + k_1'(\varepsilon_2' k' - \varepsilon_2'' k'')(k_1'^2 + k_1''^2)}{k_1' k_2'(k_2'^2 + k_2''^2)}.
\end{aligned}
$$

Therefore,

$$H_{\text{eff}}/P = \sigma_P \frac{8\alpha}{\omega} \frac{k_1' k_2' (k'k_1' + k''k_1'')(k_2'^2 + k_2''^2)}{k_2'(\varepsilon_1' k' - \varepsilon_1'' k'')(k_2'^2 + k_2''^2) + k_1'(\varepsilon_2' k' - \varepsilon_2'' k'')(k_1'^2 + k_1''^2)} \exp(-x/d_x) \exp(-|z|/d_z), \quad (A7)$$

where $d_x = 1/(2k'')$ and $d_z = 1/(2k_1')$. Due to the strong confinement in the graphene waveguide the relation $k \approx k_1 \approx k_2$ can be derived; thus Eqs. (2) and (A5) lead to

$$k \approx \frac{\pi \hbar^2 \omega^2 \varepsilon_0 (\varepsilon_1 + \varepsilon_2)[1 + i/(\tau\omega)]}{e^2} \frac{1}{\mu_c}. \quad (A8)$$

In the first-order approximation with respect to $\varepsilon_1''/\varepsilon_1'$, $\varepsilon_2''/\varepsilon_2'$, and $1/(\tau\omega)$, Eqs. (A7) and (A8) lead to

$$H_{\text{eff}}/P \approx \sigma_p \frac{8\pi^2 \hbar^4 \alpha \varepsilon_0^2 \omega^3 (\varepsilon_1' + \varepsilon_2')}{e^4} (\mu_c)^{-2}$$
$$\times \exp(-x/d_x) \exp(-|z|/d_z), \quad (A9)$$

$$d_z \approx \frac{e^2}{2\pi \hbar^2 \varepsilon_0 \omega^2 (\varepsilon_1' + \varepsilon_2')} \mu_c, \quad (A10)$$

$$d_x \approx \frac{e^2}{2\pi \hbar^2 \varepsilon_0 \omega^2 (\varepsilon_1' + \varepsilon_2')}$$
$$\times \frac{1}{[1/(\omega\tau) + (\varepsilon_1'' + \varepsilon_2'')/(\varepsilon_1' + \varepsilon_2')]} \mu_c. \quad (A11)$$

APPENDIX B: DERIVATIONS OF EQS. (7) and (8)

We start from the Lorentz reciprocity theorem [38]

$$\frac{\partial}{\partial x} \int [\vec{E}_1(\vec{r}) \times \vec{H}_2(\vec{r}) - \vec{E}_2(\vec{r}) \times \vec{H}_1(\vec{r})] \cdot \hat{x} d\sigma$$
$$= i\omega \int [\vec{E}_1(\vec{r}) \cdot \vec{D}_2(\vec{r}) - \vec{E}_2(\vec{r}) \cdot \vec{D}_1(\vec{r})] d\sigma, \quad (B1)$$

where $(\vec{E}_1, \vec{H}_1)$ and $(\vec{E}_2, \vec{H}_2)$ are two arbitrary guided modes. Now we substitute for $(\vec{E}_1, \vec{H}_1)$ and $(\vec{E}_2, \vec{H}_2)$ the unperturbed backward-propagating field $(\vec{E}^-, \vec{H}^-)$ and the perturbed forward-propagating field $(\vec{E}^p, \vec{H}^p)$ under an external transverse magnetic field, respectively. The external magnetic field $\vec{H}_{\text{ext}}$ is applied to the transverse y direction and leads to a perturbation for the mode distribution:

$$\vec{E}^- = \vec{E}^-(z) \exp(-ikx),$$
$$\vec{H}^- = \vec{H}^-(z) \exp(-ikx), \quad (B2)$$

$$\vec{E}^p = [\vec{E}(z) + \Delta\vec{E}(z)] \exp[i(k + \Delta k)x],$$
$$\vec{H}^p = [\vec{H}(z) + \Delta\vec{H}(z)] \exp[i(k + \Delta k)x]. \quad (B3)$$

In the first order of perturbation, by using Eqs. (A1), (A2), (B2), and (B3), the left side of Eq. (B1) leads to

$$\frac{\partial}{\partial x} \int [\vec{E}^-(z) \times \vec{H}(z) - \vec{E}(z) \times \vec{H}^-(z)] \cdot \hat{x} \exp(i\Delta kx) d\sigma. \quad (B4)$$

From a physical insight on backward- and forward-propagating fields, the components of the electric field and the magnetic field satisfy $E_x^-(z) = -E_x(z)$, $E_y^-(z) = E_y(z)$, $E_z^-(z) = E_z(z)$, $H_x^-(z) = H_x(z)$, $H_y^-(z) = -H_y(z)$, and $H_z^-(z) = -H_z(z)$.

Using the above relations, $[\vec{E}^-(z) \times \vec{H}(z) - \vec{E}(z) \times \vec{H}^-(z)] \cdot \hat{x} d\sigma = 2 \int [\vec{E}(z) \times \vec{H}(z)] \cdot \hat{x} d\sigma$.

The left side of Eq. (B1) is simplified as

$$2i\Delta k \exp(i\Delta kx) \int [\vec{E}(z) \times \vec{H}(z)] \cdot \hat{x} d\sigma. \quad (B5)$$

And the electric displacements are expressed as

$$\vec{D}_1 = \varepsilon_0 \varepsilon \vec{E}^-,$$
$$\vec{D}_2 = \varepsilon_0 (\varepsilon \vec{E}^p + i\alpha \vec{E}^p \times \vec{H}_{\text{ext}}). \quad (B6)$$

The right side of Eq. (B1) is

$$-\frac{k_0}{\eta_0} \int \alpha \vec{E}^- \cdot (\vec{E}^p \times \vec{H}_{\text{ext}}) d\sigma$$
$$= -\frac{2k_0}{\eta_0} \exp(i\Delta kx) \int \alpha H_{\text{ext}} E_x(z) E_z(z) d\sigma. \quad (B7)$$

Combining Eq. (B5) and Eq. (B7), we find

$$\Delta k = \frac{ik_0 \int \alpha H_{\text{ext}} E_x E_z d\sigma}{\eta_0 \int (\vec{E} \times \vec{H}) \cdot \hat{x} d\sigma}. \quad (B8)$$

Here, $(\vec{E}, \vec{H})$ is the unperturbed mode. If we assume the local magnetization response by the plasmon-induced IFE, by substituting Eq. (A6) into Eq. (B8) the nonlinear coefficient $\gamma = \Delta k/P$ is expressed as

$$\gamma = \frac{2k_0 \int \alpha^2 E_x E_z (E_x^* E_z - E_x E_z^*) d\sigma}{\eta_0^3 \int (\vec{E} \times \vec{H}) \cdot \hat{x} ds \int \text{Re}(\vec{E} \times \vec{H}^*) \cdot \hat{x} d\sigma}. \quad (B9)$$

By substituting Eqs. (A1), (A2), and (A3) into Eq. (B9), we get

$$\gamma = \frac{4\alpha^2}{\eta_0 k_0} \frac{k_1^2 k_2^3 k_1' k_2' |k_2|^2 (k_1^* k + k_1 k^*)}{(\varepsilon_1 k_2^3 + k_1^3)(k_2' |k_2|^2 \text{Re}(k\varepsilon_1^*) + k'^2 |k_1|^2)(k_1 + k_1')} \quad (B10)$$

for the scheme of Fig. 1(a) and

$$\gamma = \frac{2\alpha^2}{\eta_0 k_0 \varepsilon_1} \frac{k_1^2 k_1' (k_1^* k + k_1 k^*)}{\text{Re}(\varepsilon_1^* k)(k_1 + k_1')} \quad (B11)$$

for the scheme of Fig. 1(b). By substituting Eq. (A8) into Eqs. (B10) and (B11), we get

$$\gamma \approx \frac{4\pi^3 \hbar^6 \varepsilon_0^4 c^2 \alpha^2 \omega^5}{e^6} (\varepsilon_1' + 1)$$
$$\times \left[1 + i \left(\frac{3}{2\omega\tau} + \frac{\varepsilon_1''}{\varepsilon_1' + 1} \right) \right] (\mu_c)^{-3} \quad \text{(B12)}$$

for the scheme of Fig. 1(a) and

$$\gamma \approx \frac{16\pi^3 \hbar^6 \varepsilon_0^4 c^2 \alpha^2 \omega^5}{e^6} \varepsilon_1' \left[1 + i \left(\frac{3}{2\omega\tau} + \frac{\varepsilon_1''}{\varepsilon_1'} \right) \right] (\mu_c)^{-3}$$
$$\text{(B13)}$$

for the scheme of Fig. 1(b).

---

[1] E. Beaurepaire, J.-C. Merle, A. Daunois, and J.-Y. Bigot, Phys. Rev. Lett. **76**, 4250 (1996).

[2] C. D. Stanciu, F. Hansteen, A. V. Kimel, A. Kirilyuk, A. Tsukamoto, A. Itoh, and T. Rasing, Phys. Rev. Lett. **99**, 047601 (2007).

[3] A. Kirilyuk, A. V. Kimel, and T. Rasing, Rev. Mod. Phys. **82**, 2731 (2010).

[4] G. Armelles, A. Cebollada, A. García-Martín, and M. U. González, Adv. Opt. Mater. **1**, 10 (2013).

[5] I. S. Maksymov, Nanomaterials **5**, 577 (2015).

[6] V. V. Temnov, G. Armelles, U. Woggon, D. Guzatov, A. Cebollada, A. García-Martín, J. M. García-Martín, T. Thomay, A. Leitenstorfer, and R. Bratschitsch, Nat. Photonics **4**, 107 (2010).

[7] V. Belotelov, L. Kreilkamp, I. Akimov, A. Kalish, D. Bykov, S. Kasture, V. Yallapragada, A. V. Gopal, A. Grishin, S. Khartsev, M. Nur-E-Alam, M. Vasiliev, L. Doskolovich, D. Yakovlev, K. Alameh, A. Zvezdin, and M. Bayer, Nat. Commun. **4**, 2128 (2013).

[8] K.-S. Ho, S.-J. Im, J.-S. Pae, C.-S. Ri, Y.-H. Han, and J. Herrmann, Sci. Rep. **8**, 10584 (2018).

[9] J.-S. Pae, S.-J. Im, K.-S. Ho, C.-S. Ri, S.-B. Ro, and J. Herrmann, Phys. Rev. B **98**, 041406(R) (2018).

[10] V. I. Belotelov, E. A. Bezus, L. L. Doskolovich, A. N. Kalish, and A. K. Zvezdin, J. Phys.: Conf. Ser. **200**, 092003 (2010).

[11] S. Hamidi, M. Razavinia, and M. Tehranchi, Opt. Commun. **338**, 240 (2015).

[12] A. Dutta, A. V. Kildishev, V. M. Shalaev, A. Boltasseva, and E. E. Marinero, Opt. Mater. Express **7**, 4316 (2017).

[13] B. C. Stipe, T. C. Strand, C. C. Poon, H. Balamane, T. D. Boone, J. A. Katine, J. L. Li, V. Rawat, H. Nemoto, A. Hirotsune, O. Hellwig, R. Ruiz, E. Dobisz, D. S. Kercher, N. Robertson, T. R. Albrecht, and B. D. Terris, Nat. Photonics **4**, 484 (2010).

[14] T. Liu, T. Wang, A. H. Reid, M. Savoini, X. Wu, B. Koene, P. Granitzka, C. E. Graves, D. J. Higley, Z. Chen, G. Razinskas, M. Hantschmann, A. Scherz, J. Stohr, A.Tsukamoto, B. Hecht, A. V. Kimel, A. Kirilyuk, T. Rasing, and H. A. Durr, Nano Lett. **15**, 6862 (2015).

[15] M. A. Kozhaev, A. I. Chernov, D. A. Sylgacheva, A. N. Shaposhnikov, A. R. Porokopov, V. N. Berzhansky, A. K. Zvezdin, and V. I. Belotelov, Sci. Rep. **8**, 11435 (2018).

[16] A. L. Chekhov, A. I. Stognij, T. Satoh, T. V. Murzina, I. Razdolski, and A. Stupakiewicz, Nano Lett. **18**, 2970 (2018).

[17] S.-J. Im, J.-S. Pae, C.-S. Ri, K.-S. Ho, and J. Herrmann, Phys. Rev. B **99**, 041401(R) (2019).

[18] S.-J. Im, C.-S. Ri, K.-S. Ho, and J. Herrmann, Phys. Rev. B **96**, 165437 (2017).

[19] M. Tonouchi, Nat. Photonics **1**, 97 (2007).

[20] B. Ferguson and X.-C. Zhang, Nat. Mater. **1**, 26 (2006).

[21] R. Soref, Nat. Photonics **4**, 495 (2010).

[22] S. A. Mikhailov and K. Ziegler, Phys. Rev. Lett. **99**, 016803 (2007).

[23] P. Avouris, IEEE J. Sel. Top. Quantum Electron. **20**, 6000112 (2014).

[24] D. A. Kuzmin, I. V. Bychkov, V. G. Shavrov, and V. V. Temnov, Nanophotonics **7**, 597 (2018).

[25] I. V. Bychkov, D. A. Kuzmin, V. A. Tolkachev, P. S. Plaksin, and V. G. Shavrov, Opt. Lett. **37**, 1895 (2018).

[26] E. D. Palik, R. Kaplan, R. W. Gammon, H. Kaplan, R. F. Wallis, and J. J. Quinn, Phys. Rev. B **13**, 2497 (1976).

[27] M. Tymchenko, A. Y. Nikitin, and L. Martín-Moreno, ACS Nano **7**, 9780 (2013).

[28] M. Jablan, H. Buljan, and M. Soljačić, Phys. Rev. B **80**, 245435 (2009).

[29] J. J. Brion, R. F. Wallis, A. Hartstein, and E. Burstein, Phys. Rev. Lett. **28**, 1455 (1972).

[30] F. Liu, C. Qian, and Y. D. Chong, Opt. Express **23**, 2383 (2015).

[31] B. Zhu, G. Ren, Y. Gao, B. Wu, Q. Wang, C. Wan, and S. Jian, Opt. Express **23**, 16071 (2015).

[32] G. Xu, M. Cao, C. Liu, J. Sun, and T. Pan, Opt. Commun. **366**, 112 (2016).

[33] D. A. Kuzmin, I. V. Bychkov, V. G. Shavrov, and V. V. Temnov, Nano Lett. **16**, 4391 (2016).

[34] J.-S. Pae, S.-J. Im, C.-S. Ri, K.-S. Ho, G.-S. Song, Y.-H. Han, and J. Herrmann, Phys. Rev. B **100**, 041405(R) (2019).

[35] A. K. Zvezdin and V. A. Kotov, *Modern Magnetooptics and Magnetooptical Materials* (IOP, Bristol, England, 1997).

[36] Y. Gao, G. Ren, B. Zhu, H. Liu, Y. Lian, and S. Jian, Opt. Express **22**, 24322 (2014).

[37] X. Lin, Z. Wang, F. Gao, B. Zhang, and H. Chen, Sci. Rep. **4**, 4190 (2014).

[38] A. Snyder and J. D. Love, *Optical Waveguide Theory* (Chapman & Hall, London, 1983).

[39] B. Wang, X. Zhang, F. J. Garcia-Vidal, X. Yuan, and J. Teng, Phys. Rev. Lett. **109**, 073901 (2012).

[40] A. Vakil and N. Engheta, Science **332**, 1291 (2011).